Journal Name

ARTICLE

Uptake and transcytosis of functionalized superparamagnetic iron oxide nanoparticles in an *in vitro* blood brain barrier model

Received
Accepted

DOI: 10.1039/x0xx00000x

www.rsc.org/

Angela Ivask[a,b*], Emily H. Pilkington[c], Thomas Blin[c], Aleksandr Käkinen[c], Heiki Vija[b], Meeri Visnapuu[b,d], John F. Quinn[c], Michael R. Whittaker[c], Ruirui Qiao[c], Thomas P. Davis[c,e], Pu Chun Ke[c*] and Nicolas H. Voelcker[a,f-j*]

Two major hurdles in nanomedicine are the limited strategies for synthesizing stealth nanoparticles and poor efficacy of the nanoparticles in translocating across the blood brain barrier (BBB). Here we examined the uptake and transcytosis of iron oxide nanoparticles (IONPs) grafted with biomimetic phosphorylcholine (PC) brushes in an *in vitro* BBB model system, and compared it with bare, PEG or PC-PEG mixture grafted IONPs. Hyperspectral imaging indicated IONP co-localization with cells. Quantitative analysis with total reflection X-ray fluorescence spectrometry showed that after 24 h, 78% of PC grafted, 68-69% of PEG or PC-PEG grafted, and 30% of bare IONPs were taken up by the BBB. Transcytosis of IONPs was time-dependent and after 24 h, 16-17% of PC or PC-PEG mixture grafted IONPs had passed the model BBB, significantly more than PEG grafted or bare IONPs. These findings point to PC as a viable grafting strategy for the uptake and transcytosis of nanoparticles.

Keywords: IONPs, *in vitro* BBB model, cellular internalization, transcytosis

Introduction

Superparamagnetic iron oxide nanoparticles (IONPs) represent a promising class of nanomaterials for biomedical applications owing to their biocompatibility, tuneable size and surface functionality, as well as flexibility in the control of their biodistribution and pharmacokinetics.[1] Indeed, the physical properties of IONPs have been exploited for magnetic resonance imaging (MRI) and thermoablation therapy, while the ease of surface conjugation of IONPs is attractive for cell targeting. Unlike gadolinium- and iodine-based MRI, X-ray and computed tomography agents that are cleared by kidneys to evoke toxicity, iron oxides are likely to enter the body's iron cycle.[2]

For better biocompatibility and prolonged blood circulation in biological systems, IONPs are usually coated or grafted with hydrophilic polymers such as polyethylene glycol (PEG).[3-5] PEG, either in the linear or brushed form, resists protein adsorption by steric repulsion (for flexible PEG chains) or hydrogen bonding with water (for inflexible PEG chains).[6,7] Consequently, PEGylation is the most common antifouling strategy against formation of the protein corona[8,9] and in conferring a stealth effect to nanoconstructs in biomedical and biotechnological applications.[7] However, despite its low toxicity, simple chemistry and commercial success, PEG is non-biodegradable and may accumulate *in vivo,* and the potential effect from such accumulation is largely unknown.[9] The recent proteomic identifications of the associations of PEGylated polymeric and gold NPs with apolipoproteins A-1 and E as well as complement proteins[10-12] highlight the potential immunological and pathological drawbacks of this major grafting strategy.

Phosphorylcholine (PC), the hydrophilic polar head group of phospholipids has been considered as an alternative stealth material.[13-15] We have recently demonstrated a novel strategy of grafting IONPs with poly(2-(methacryloyloxy)ethyl phosphorylcholine) (poly(MPC)) brushes *via* a phosphonic acid linker.[16] Coating of IONPs with poly(MPC) brushes afforded similar or enhanced stability, stealth effect,[7] biocompatibility and cellular distribution compared with PEG coatings. To facilitate the continued development of alternative strategies for MRI applications, here we

[a] *ARC Centre of Excellence in Convergent Bio-Nano Science and Technology, Future Industries Institute, University of South Australia, Mawson Lakes, SA, Australia*
[b] *Laboratory of Environmental Toxicology, National Institute of Chemical Physics and Biophysics, Tallinn, Estonia*
[c] *ARC Centre of Excellence in Convergent Bio-Nano Science and Technology, Monash Institute of Pharmaceutical Sciences, Monash University, Parkville, VIC, Australia*
[d] *Institute of Physics, University of Tartu, Tartu, Estonia*
[e] *Department of Chemistry, University of Warwick, Gibbet Hill, Coventry, United Kingdom*
[f] *Drug Delivery, Disposition and Dynamics, Monash Institute of Pharmaceutical Sciences, Monash University, Parkville, Victoria, Australia*
[g] *Melbourne Centre for Nanofabrication, Victorian Node of the Australian National Fabrication Facility, Clayton, Victoria, Australia*
[h] *Commonwealth Scientific and Industrial Research Organisation (CSIRO), Clayton, Victoria, Australia*
[i] *Monash Institute of Medical Engineering, Monash University, Clayton, Victoria, Australia*
[i] *INM-Leibniz Institute for New Materials, Saarbrücken, Germany*

Corresponding email addresses: angela.ivask@kbfi.ee; pu-chun.ke@monash.edu; nicolas.voelcker@monash.edu

Electronic Supplementary Information (ESI) available: [details of any supplementary information available should be included here]. See DOI: 10.1039/x0xx00000x

characterized the uptake of IONPs grafted with poly(MPC) brushes[16] in cerebral endothelial cells, and transcytosis of those NPs through a model blood brain barrier (BBB)[17], in comparison to PEG-grafted IONPs. The BBB regulates the transport of nutrients and biomolecules to the brain and is considered one of the most impermeable biological barriers. Therefore, efficient translocation of drugs and NPs through the BBB is a paramount challenge in nanomedicine and improvements in this aspect are of great importance.

Materials and Methods

Synthesis and characterizations of IONPs. IONPs synthesized and tested in the current study are shown in Fig. 1 and Table 1.

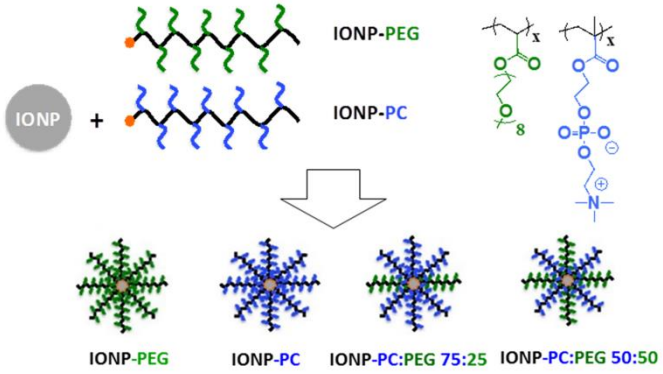

Fig. 1. Schemes of IONPs grafted with brushed PC, PEG, as well as with 75:25 and 50:50 brushed PC and PEG.

Table 1. Description and characteristics of the IONPs

	Surface characteristics	Dh in water (nm)	Dh in cell culture medium (nm)
bare IONPs	No surface functionalization	323±9.8 [c]	340±16 [d]
IONP-PEG	poly(OEGA)	141±0.7 [a]	151±1.4 [c]
IONP-PC	poly(MPC)	121±0.7 [a]	112±2.0 [c]
IONP PC:PEG 75:25	poly(OEGA) and poly(MPC)75:25 molar ratios	105±0.6 [a]	103±0.3 [a]
IONP PC:PEG 50:50	poly(OEGA) and poly(MPC)50:50 molar ratios	112±1.1 [a]	126±2.5 [a]

Dh – hydrodynamic diameter; [a]-polydispersity index (PDI) <0.2, [b]-PDI 0.2-0.3, [c]-PDI 0.3-0.4, [d]-PDI >0.4

The detailed synthesis of IONPs coated with PC, PEG or PC-PEG mixtures is described in our recent publication.[16] For transmission electron microscopy (TEM), 5 µL aliquot of 50 µg/mL IONPs was dropped onto copper grids (300 mesh, GCu300, ProSciTech), allowed to adsorb for 5 min and then air-dried. The samples were examined by TEM (JEOL JEM-2100F) at 200 kV. The hydrodynamic diameters (Dh) of the IONPs (10 µg/mL suspensions) were determined by dynamic light scattering (DLS) (Nano ZS, Malvern) in three parallels. Particle size distribution and polydispersity index (PDI) were analyzed using Malvern Zetasizer software.

Cell culture. Human cerebral endothelial cell line hCMEC/D3[17] was from Cedarlane. This is an established cell line for modelling the BBB as it maintains a contact-inhibited monolayer, exhibits robust proliferation in response to endothelial growth factors, and grows indefinitely without phenotypic de-differentiation.[17] This model system has been employed to study the transport of pathogens,[18] drugs[19] and NPs[20-23] through the BBB. hCMEC/D3 cells were grown at 37° C with 5% CO_2 on collagen I-coated cell culture flasks, membranes and coverslips (0.01% collagen I, Sigma, in 10 mM acetic acid for 30 min). The cell growth and exposure medium was EBM-2 medium (Lonza) supplemented with 10 mM HEPES (Sigma), 1% penicillin-streptomycin (Sigma), 5 µg/mL ascorbic acid (Sigma), 1.4 µM hydrocortisone (Sigma), 5% FBS (Hyclone), 1% chemically defined lipid concentrate (Gibco), and 1 ng/mL basic fibroblast growth factor (Sigma). The cells were kept at a passage number between 25 and 35 and the cell density on culture dishes between 2×10^5 and 1×10^6 cells/mL.

Neutral red uptake assay for cytotoxicity. A neutral red *in vitro* toxicology assay kit (Sigma) was used to determine IONP-induced cytotoxicity. hCMEC/D3 (seeded at 5×10^4 cells/mL) were exposed to 0.002-1 pM (0.5-100 µg/mL) IONPs/mL on 96-well plates and the assay was carried out per Sigma protocol (see Supporting Information or SI).

Laurdan assay for cell membrane fluidity. The assay was carried out according to Owen et al. [24] 5×10^5 hCMEC/D3 cells/mL were seeded to collagen I-coated 0.17 µm coverslips (Zeiss), allowed to attach over 24 h, and exposed to 50 µg/mL (~0.5 pM) IONPs for 24 h. After that 5 µM Laurdan dye (6-lauryl-2-dimethylamino-napthalene) diluted in cell culture medium was added and cells were incubated for 30 min at 37° C and 5% CO_2. Coverslips with cells were mounted using Fluoro Gel with DABCO on microscope slides and imaged with confocal fluorescence microscopy (Elyra, Zeiss) using 405 nm/430-470 nm or 480-550 nm for gel/liquid ordered membrane channel and liquid disordered membrane channel, respectively. The images were saved as 64-bit TIFF and the generalized polarization (GP) values of the membrane pixels were calculated[25] (see SI).

Hyperspectral imaging of IONP-exposed cells. hCMEC/D3 cells were grown on coverslips and exposed to 50 µg/mL (~0.5 pM) IONPs as above. After exposure, the growth medium was discarded, the cells were washed with PBS and fixed with 4% formaldehyde solution (Sigma) for 10 min. The coverslips were mounted on microscope slides and the cells were imaged by a dark-field hyperspectral microscope (CytoViva). ENVI 4.8 (CytoViva) was used for data analysis and identification of IONPs in cells[16] (see SI).

Growing and imaging cells on transwell membranes. 2×10^5 hCMEC/D3 cells/mL were seeded to collagen I-treated transwell permeable supports (Corning, 6.5 mm diameter) with 3.0 µm pore size membranes that were placed into 24-well plates. The cells were allowed to grow for 13 d and the transepithelial electrical resistance (TEER) was measured daily or every 2 d using a Millicell® ERS-2 Voltohmmeter (Merck Millipore). The TEER value of the medium was registered and subtracted as the background from the values measured in cell-containing transwell inserts. For staining, the 6 d grown cells on transwell membranes were rinsed with PBS and fixed

with 4% formaldehyde for 10 min, rinsed with PBS and incubated with 0.1% Triton X-100 for 5 min. Then the cells were incubated with 0.16 µM rhodamine (TRITC) phalloidin (ThermoFisher) in PBS for 20 min and 0.2 µg/mL Hoechst 33342 (ThermoFisher) in PBS for 10 min. Images were taken using confocal fluorescence microscopy (Zeiss Elyra, 405, 488 and 530 nm) with a 63× water-immersion objective. 3D images were constructed from z-stacks of 0.4 µm between individual layers.

Imaging IONP exposed cells using transmission electron microscopy. hCMEC/D3 monolayers grown on transwell membrane as above and exposed to 50 µg/mL of the different versions of IONPs for 24 h were prepared for TEM using a modified protocol from Schrand *et al.*[26] Detailed sample descriptions are given in the SI. Ultrathin sections were prepared by Leica EM UC7 and the sections were viewed using Tecnai G2 Spirit BioTwin at 120 kV.

Translocation of IONPs through hCMEC/D3 cell monolayer. 6-d confluent layers of hCMEC/D3 cells on transwell membranes were exposed to 50 µg/mL (~0.5 pM) of the different versions of IONPs. 180 µL of IONPs suspended in cell culture medium was added to the apical side (mimicking the bloodstream, i.e., luminal side) of the transwell system and 700 µL of cell culture medium (without IONPs) was pipetted to the lower, basolateral layer (eventually, brain side, i.e., abluminal side). The cells were incubated for 1, 4 or 24 h after which samples from the apical (blood side) and basolateral (brain side) layers were collected. Next, the cell monolayer on the membranes was removed by adding 100 µL trypsin-EDTA (Sigma), incubating for 15 min at 37° C, addition of 100 µL of cell culture medium followed with resuspension. 7% HNO_3 was added to all collected samples. In addition, the membranes were cut out and exposed to 7% HNO_3 overnight to remove membrane-bound residual IONPs. In parallel to transwell membranes with cell monolayers, we also determined the translocation of IONPs through transwell membranes lacking a cell monolayer. In this case, only samples from the apical and basolateral layers were collected and membrane-bound IONPs were collected. The Fe concentration in the samples was analyzed using total reflection X-ray fluorescence (TXRF) (Picofox S2, Bruker) as described in reference 16. Briefly, the collected samples were sonicated (Branson Model 450 with a microtip, 5% power) for 10 s, 40 µL of each sample was mixed with 40 µL of the reference element (Ga, at 2 mg/L in 1% HNO_3) and 3 µL of the sample was pipetted into a quartz sample holder (Analyslide Petri Dish, Pall). The sample was dried at 60° C and fluorescence was measured for 600 s. Fe concentration was calculated according to the Ga standard. Cell media without IONPs were used to determine the media background at 0.29±0.03 µg/mL of Fe. All results from IONP exposures were significantly ($p < 0.05$) higher than the media background.

Replicates and statistical analysis. At least 3 independent replicates were performed for each sample condition. IONP translocation was analyzed using one-way ANOVA: Post Hoc Multiple Comparisons (Tukey) in SPSS software (IBM). $p < 0.05$ (i.e., 95%) differences between different treatments were considered as statistically significant.

Results

Characterization of IONPs. TEM images and hydrodynamic size of the five types of IONPs with different surface functionalities (Table 1) are shown in Fig. 2. The primary size of all the IONPs variants was ~15 nm. Overall, the dispersibility of all samples was good with a polydispersity index<0.4 (Table 1) in water and slightly above 0.4 in cell culture medium. Although the IONP cores were identical, the Dh of the IONPs varied. Specifically, bare IONPs possessed the largest average hydrodynamic size, 323 nm in water and 340 nm in cell culture medium, and PC, PEG and PC:PEG mixture coated IONPs exhibited significantly lower average Dh values (between 102 and 151 and 250 nm) and thus, better suspension stability (Fig. 2).

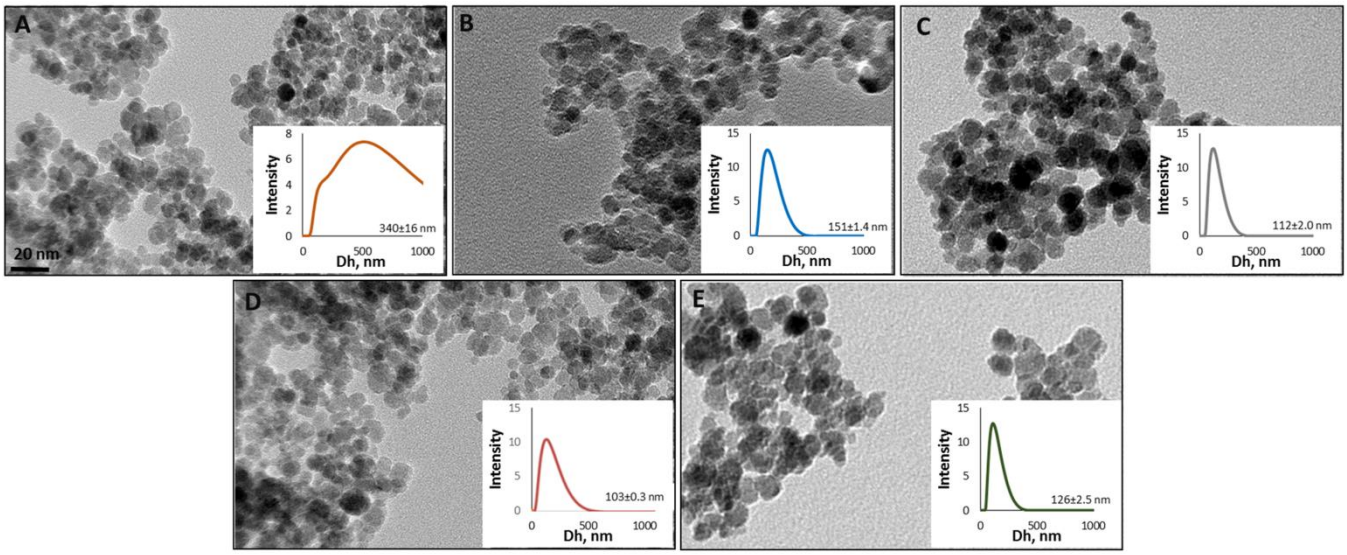

Fig. 2. TEM images of (A) bare IONPs, (B) IONP-PEG, (C) IONP-PC, (D) IONP-PC:PEG 75:25 and (E) IONP-PC:PEG 50:50. The scale bar in (A) applies to all panels. The insets show the hydrodynamic diameter (Dh) of IONPs in cell culture medium. Average Dh values with standard deviations are shown.

Cytotoxicity of IONPs to human cerebral endothelial cells. To keep the integrity of hCMEC/D3 BBB model during nanoparticle incubation, the toxicities of the IONPs with different surface capping agents were evaluated. As shown in Fig. 3A no significant loss in

cellular viability was observed for exposures up to 1 pM (100 µg/mL) (Fig. 3A). Therefore, 0.5 pM (50 µg/mL) – a concentration of IONPs not affecting cellular viability, was chosen for further studies on cellular uptake and BBB transport.

In addition to cytotoxicity, the effect of IONP exposure on cell membrane fluidity was evaluated. Laurdan, a dye which upon an increase in membrane fluidity, undergoes a spectral redshift [24] was employed as a reporter dye for temporary changes in the membranes of 0.5 pM IONP exposed cells. Compared to non-exposed cells, IONP-exposed hCMEC/D3 cells exhibited increased generalized polarization values indicating a relatively high fraction of ordered bilayer membrane (Fig. 3B). Thus, exposure of cells to IONPs, most notably for IONP-PC and least for bare IONPs, induced a significant reduction in membrane fluidity compared to non-exposed cells.

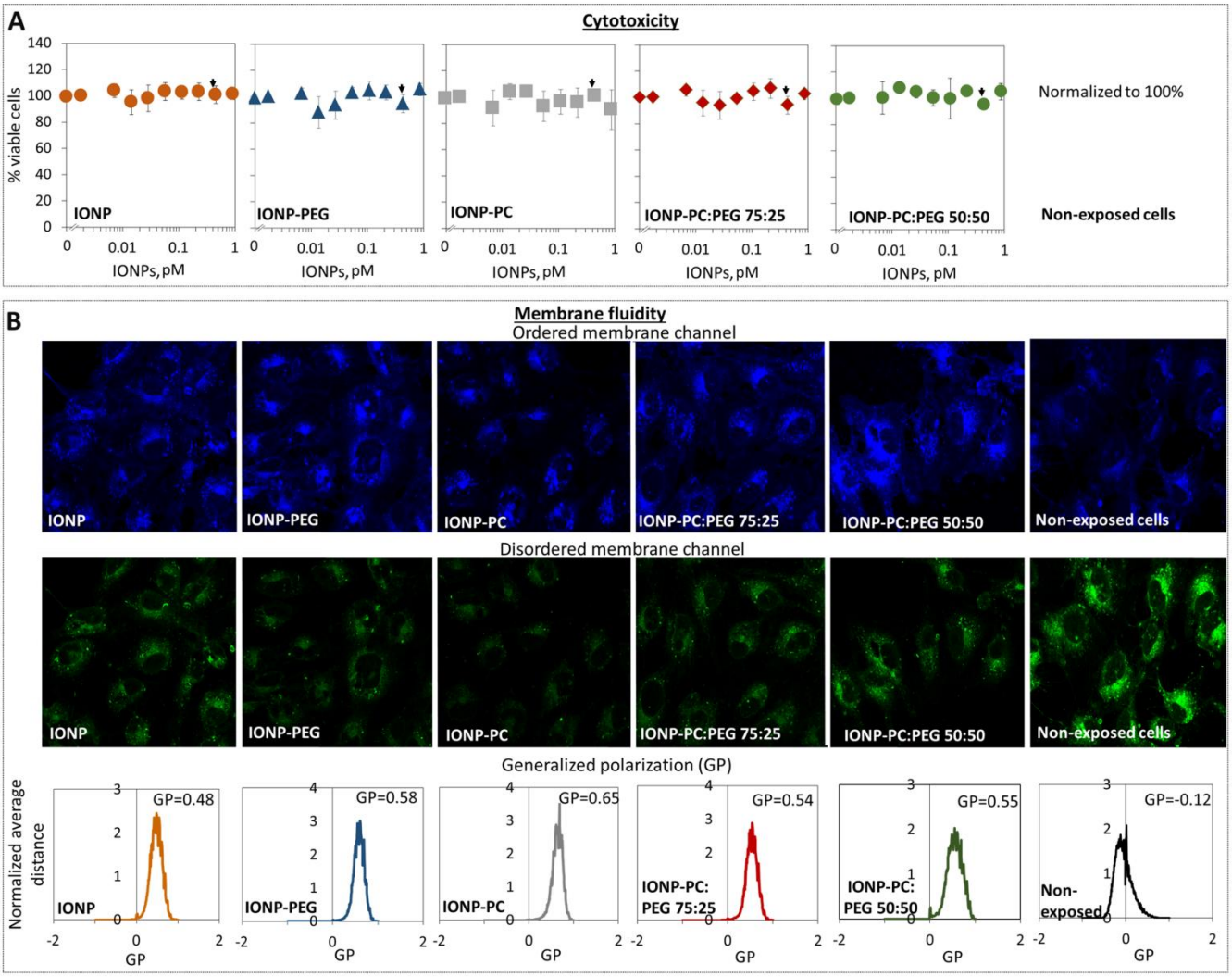

Fig. 3. (A) Cytotoxicity of IONPs to hCMEC/D3 cells over 24 h, measured with neutral red uptake assay; non-exposed cells were considered 100% viable. Down pointing arrows indicate 50 µg/mL (~0.5 pM) concentration that was used in cellular uptake and BBB translocation tests. (B) Membrane fluidity of cells exposed to 50 µg/mL IONPs for 24 h, showing representative fluorescence images of ordered and disordered membrane channels and their generalized polarization (GP) values. Increases in GP indicate decreased membrane fluidity.

Journal Name

ARTICLE

The interactions between IONPs and hCMEC/D3 cells were further examined using dark field and hyperspectral imaging (Fig. 4). Upon 24-h exposure to 0.5 pM IONPs, all IONP types were co-localized with the cells (NPs shown as bright pixels in Fig. 4A-E). The peak scattering wavelengths of the cell-associated aggregates were between 450 and 650 nm (Fig. 4F), close to the absorbance spectrum of IONPs. Collectively, these experiments verified cellular interactions and potential uptake of the IONPs by the BBB model cells.

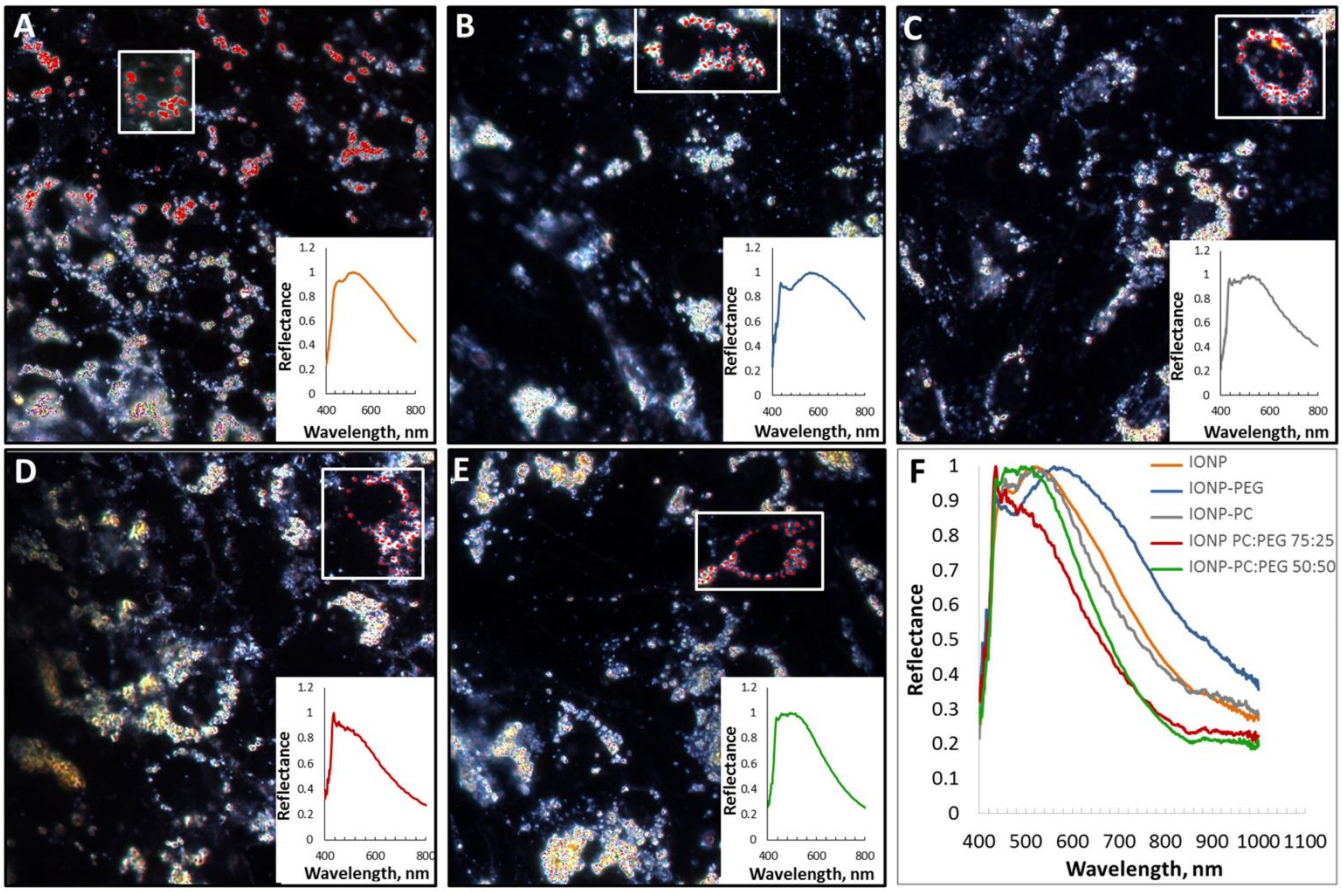

Fig. 4. Cells exposed to 50 µg/mL of (A) bare IONPs, (B) IONP-PEG, (C) IONP-PC, (D) IONP-PC:PEG 75:25 and (E) IONP-PC:PEG 50:50. For each image, background (of non-exposed cells) was subtracted and one cell shown inside a square was selected to identify the characteristic spectra of IONPs (selected pixels shown in red). The characteristic reflectance spectra are shown in insets of A-E and combined in panel F. The presence of the characteristic spectra in the rest of the images was identified (colored pixels in A-E).

Translocation of IONPs across a model BBB. Ta quantitatively assess the cellular uptake and translocation of IONPs in BBB model, hCMEC/D3 cerebral endothelial cells were grown on 3 µm transwell membranes to confluent layer and exposed to 0.5 pM (50 µg/mL) of each IONP. In order to monitor the integrity of the *in vitro* BBB before the test with NPs, cell growth and monolayer formation on transwell membranes were examined using TEER measurement and microscopy. The TEER measurement showed an increased electrical resistance up to 60 Ω/cm^2 at day 6, after which no significant increase in resistance was observed (Fig. S1A). Therefore, 6 d was selected as an optimal time for cell monolayer formation on the transwell system. Visual representation of a 6-d cell monolayer on membranes is given in Fig. S1B-D, and the presence of mature tight junctions (TJ) in cell monolayer (vascular endothelial cadherin, one of the TJ components) is shown in Fig. S2C.

Journal Name

ARTICLE

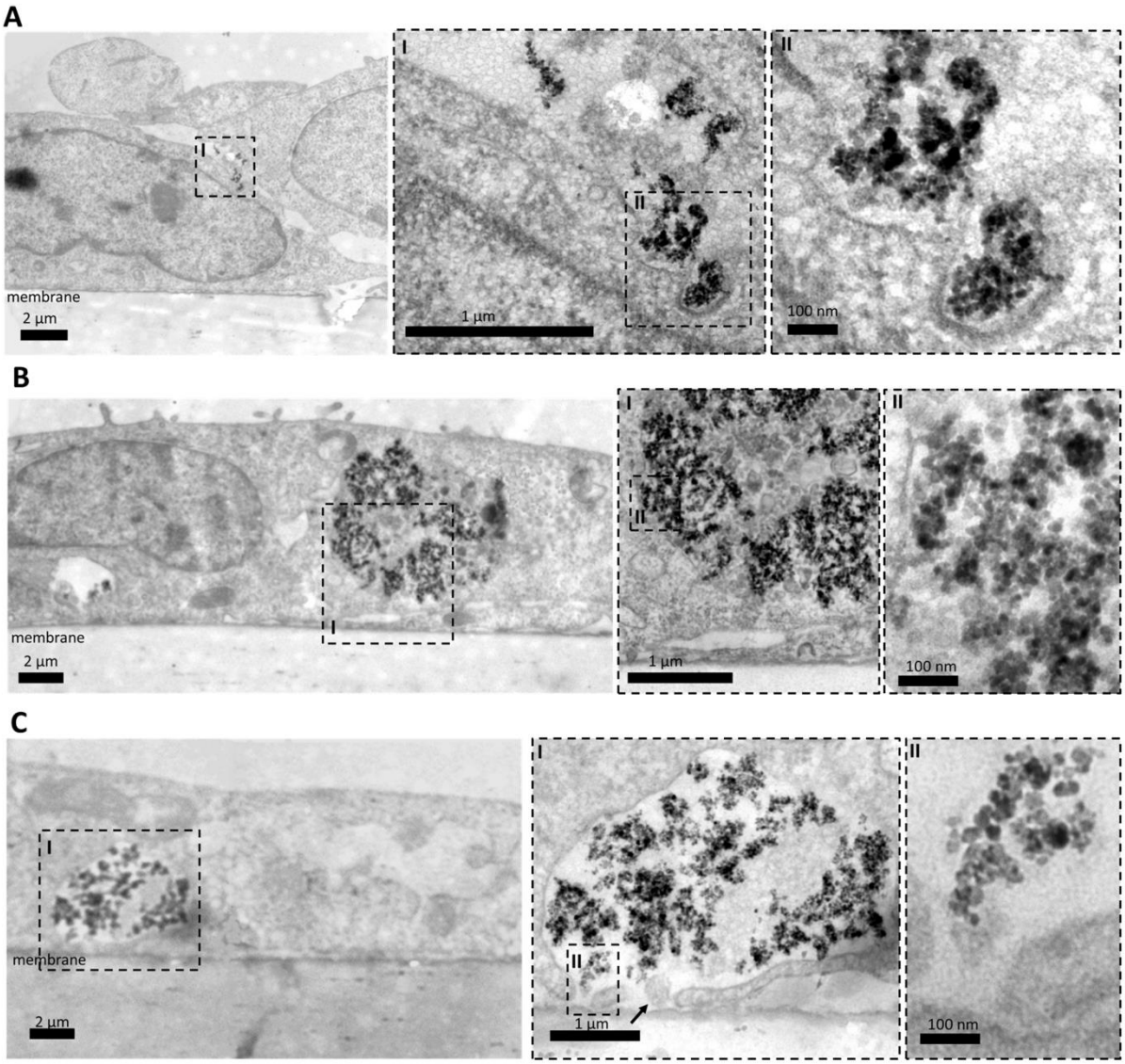

Fig. 5. Localization of IONPs in hCMEC/D3 cell layer on transwell membrane under TEM. The cell monolayer on transwell membranes was exposed to 50 µg/mL IONPs. Selected images show an early endocytotic vesicle in (A) IONP-PC:PEG 75:25 exposed cells, (B) a late endocytotic vesicle in IONP-PC:PEG 50:50 exposed cells and (C) exocytotic vesicle on the basolateral side of IONP-PEG exposed cells. Insets I and II in each panel are enlarged views of regions indicated with dashed lines. Images of cells exposed to all variants of IONPs are shown in Fig. S3.

Prior to quantitative analysis of IONP translocation, intracellular localization and trafficking of IONPs through the cell layer was imaged with TEM. For all IONP exposures, NPs were observed in endocytotic vesicles in hCMEC/D3 cells (Fig. S3) and the presence of Fe in the vesicles was proven with energy dispersive X-ray (EDX) analysis (Fig. S3D). Fig. 5A-C show representative images of NPs taken up by the cells to endocytotic vesicles from the apical side, NPs in a vesicular structure inside the cells and NPs exocytosed by the cells to the basolateral side of the cell layer. For quantitative analysis of cellular translocation of IONPs in the *in vitro* BBB model, the Fe content was quantified on apical, basolateral and cell layers using TXRF. To first characterize the kinetics of BBB translocation, the fractions of IONP-PEG in the apical, basolateral sides and cell monolayer after 1, 4 and 24 h of exposure were analyzed (Fig. 6B). One hour of exposure was enough for 13% of the added NPs to associate with the monolayer and 0.17% of the added NPs to translocate through the BBB model. After 4 h, 22% of the added NPs were associated with BBB and 3.5% of the added NPs translocated

across the barrier, and after 24 h, 68% of the particles were associated with the cells and 15% passed the cell layer. In comparison, for transwell membranes lacking the cell monolayer, the maximum translocation of IONP-PEG was achieved within 4 h (Fig. S4).

In 24 h nanoparticle exposed cells, clear differences in quantities of Fe in the studied layers were observed for IONPs with different surface functionalities (Fig. 6). The most significant difference between the different IONPs was their partitioning in the hCMEC/D3 cell monolayer, i.e., 30% of bare IONPs, 68% of IONP-PEG, 69% of IONP-PC:PEG 75:25 and IONP PC:PEG 50:50 and 78% of IONP-PC were co-localized with the cells, respectively (Fig. 6E). This is a strong indication of better association of functionalized IONPs compared to bare IONPs with the model BBB. These data also show that PC surface functionality enabled significantly better cellular contact and uptake compared with PEG surface coating (Fig. 6).

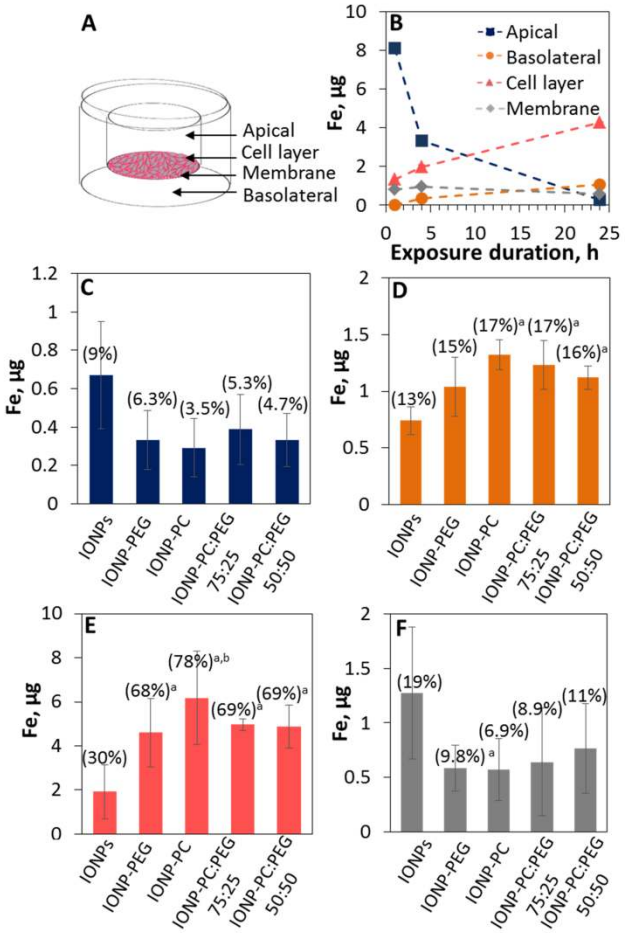

Fig. 6. Transport of IONPs in transwell system with hCMEC/D3 cell layer. (A) Schematic representation of the transwell system. A 6 d grown cell monolayer on the transwell membrane was exposed to 50 µg/mL of the different types of IONPs that were introduced from apical side; Fe concentrations in apical and basolateral sides, in cell layer, and in membrane were quantified using TXRF. (B) Time-dependent localization of IONP-PEG in different compartments of the transwell system. Localization of IONPs with different coatings in (C) apical and (D) basolateral side, (E) cell monolayer or (F) on the membrane after 24 h exposure. Means and standard deviations of three independent experiments are shown, [a] – significant ($p < 0.05$) difference between IONPs and IONPs with PEG, PC coatings, or mixture coatings; [b] - significant ($p < 0.05$) difference between IONP-PEG and IONP-PC, IONP-PC:PEG 75:25 or IONP-PC:PEG 50:50. In panels C-F the percentages of introduced IONPs are shown.

We acknowledge that the fraction of IONPs that was co-localized with the cell monolayer could include both cell-membrane-associated NPs as well as those endocytosed by the cells. But since the cell monolayer was carefully rinsed before its digestion and the IONPs were visualized inside the cells after 24-h exposure most of the cell-associated NPs were likely localized inside the hCMEC/D3 cells.

TXRF analysis of the Fe concentration in the basolateral layer of the BBB model, i.e., the side representing the brain, showed that IONP-PC and IONP-PC:PEG 75:25 transcytosed through the model BBB significantly ($p < 0.05$) more efficiently than bare IONPs (Fig. 6D). In the case of bare IONPs, 13% of the added NPs were detected in the basolateral layer whereas in the case of IONP-PC and IONP-PC:PEG 75:25 17% of the NPs were transported to the basolateral side (Fig. 6D). Transcytosis of IONP-PEG and IONP-PC:PEG 50:50 was 15 and 16%, respectively and did not statistically differ from that of bare IONPs. Thus, there was a notable improvement in transcytosis for PC-functionalized particles compared with PEG-coated ones.

Discussion

This study aimed to characterize the cellular uptake and translocation of IONPs with different surface grafting agents (Table 1; Fig. 1) with an *in vitro* hCMEC/D3 BBB model. All the tested IONPs proved non-toxic up to 100 µg/mL to the BBB model, consistent with previous observation with human embryonic kidney cells.[16] IONP-exposed cells (Fig. 3) showed increased membrane ordering (decreased fluidity), following the sequence of bare IONPs, IONP-PEG, IONP-PC:PEG 50:50, IONP-PC:PEG 75:25, and IONP-PC. Decreased membrane fluidity upon NP exposure has been reported in previous studies.[27] Using computer simulations, Mhashal and Roy[28] also showed that gold NPs coming into contact with or penetrating into a lipid bilayer gave rise to local membrane deformations and enhanced local lipid ordering, thereby decreasing the bilayer fluidity. We therefore infer that the increasing ordering in IONP-exposed cell membranes was an indicator of cellular binding or uptake of the IONPs. Co-localization of IONPs with cells was validated by hyperspectral imaging (Fig. 4).

To enable the major application of IONPs as MRI contrast agents in brain imaging, we analyzed the potential of IONPs to translocate through a model *in vitro* BBB – a monolayer of hCMEC/D3 cerebral endothelial cells grown for 6 d on 3 µm pore size membranes on transwell plates (Fig. S1B-D). Pore size of 3 µm was selected since earlier studies indicated blockage of smaller (0.4 µm) pores by 50 nm SiO_2 NPs.[23] The 3 µm pore size membranes (empty membranes with no cells) allowed the transloaction of ~50% of the IONPs (IONP-PEG were used as an example) through the membranes within 4 h, and only a slight increase up to 55% was observed when exposure was prolonged to 24 h (Fig. S4B). Thus, after at least 4 h, the IONP concentrations on both slides of the membrane were equalized and the NPs were moving freely in the empty transwell system.

The integrity of 6 d hCMEC/D3 cell monolayer on transwell membranes was assured by TEER, which showed an electrical resistance of 60 Ω/cm^2 (Fig. S1A), an improvement over the previously reported values of 30-50 Ω/cm. [17] While this TEER value is relatively low compared to what could be expected *in vivo*[17], and certain imperfections (areas with bi-or multilayers of cells, holes or

gaps may remain on the membranes[22]) cannot be excluded, the transwell set-up has been used in a number of studies[20-23] and is a well-established method.[23] We stained the 6 d hCMEC/D3 cell monolayer with vascular endothelial cadherin (one of the TJ components) antibody and subsequent fluorescent staining indicated that TJs had formed over most of the observed area (Fig. S2C). The latter proved the integrity of the 6-d grown BBB model.

When the model BBB system was exposed to IONPs for 24 h and cells were observed by electron microscopy, IONPs were observed in endocytotic vesicles in all exposures (Fig. S3). Transcytosis was also observed as shown in Fig. 5. As proven by EDX analysis, particulates observed in endocytotic vesicles contained Fe (Fig. S3D).

It is interesting to note that there are only a few studies available where translocation of NPs through BBB has been quantitatively studied,[20,22,23,29] and all these studies relied on measuring the fluorescence of specifically tagged NPs. Here the transcytosis efficacy of IONPs was quantified with TXRF. We observed that the transport of IONPs in the BBB model differed between the different types of IONPs. Bare IONPs had clearly lower presence in the cell layer and basolateral (brain side) layer than the surface-coated IONPs, while higher concentration of bare IONPs was present in apical (blood side) layer. Among different coatings, PC-coated IONPs were clearly present at the highest concentrations in the cell layer (78%) and the basolateral layer (17%) (Fig. 6D and E). Thus, PC may be as an alternative and improved grafting strategy for the optimal BBB transport of IONPs. While our transcytosis efficacy of IONPs ranged from 13 to 17%, Thomsen et al.[30] showed that transcytosis of 118 nm uncoated IONPs was ~6% (3-4 µg/mL IONPs transported at 60 µg/mL exposure concentraion), Bramini et al.[22] demonstrated that 24 h exposure of a model BBB resulted in the passage of ~7% of carboxy-modified polystyrene particles and Georgieva et al.[21] showed that, depending on surface properties, 2-10% of SiO_2 NPs translocated through the cell layer. This latter study also reported that 60-90% of differently coated SiO_2 NPs remained bound with the BBB cell layer – a value that is similar to our measurement for surface functionalized IONPs (Fig. 6E).

Although the uptake and transcytosis of NPs in BBB model systems has been examined by several studies, the mechanisms behind those processes remain somewhat unclear. Ye et al.[29] studied the uptake, accumulation and transcytosis of SiO_2, TiO_2 and Au NPs through the layers of hCMEC/D3 and found that the NPs in general accumulated in cells via the endo-lysosomal pathway. Georgieva et al.[21] demonstrated that endocytosis of NPs by BBB cells depended on particle surface coating and the main pathways were caveolae-mediated endocytosis and micropinocytosis. Exposure of BBB layers to NPs (SiO_2 and quantum dots) caused loss of TJs between the cells and thinning of the cell layer,[20] which could be an additional mechanism enabling translocation of NPs through the endothelial cell layer. One of the translocation pathways that NPs are likely to use in BBB could be adsorptive-mediated transcytosis which takes place via clathrin-mediated vesicles or caveolae.[31, 32] This transcellular transport mechanism may start by random uptake of molecules (or particles) in luminal space or specific interaction of the molecules with negatively charged clathrin-coated pits near the membrane of endothelial cells. [31] It should be however mentioned that the transcytosis efficacy of BBB is orders of magnitude lower compared to any other endothelial layer[32] which suggests that the fraction of transcytosed NPs can be relatively low. Hanada et al.[20] calculated the translocation efficacy of NPs through their model BBB and found it to depend greatly on particle concentration. For example, permeability coefficient (P_{app}) for 30 nm SiO_2 NPs varied from 1×10^{-6} cm/s to 4×10^{-6} cm/s depending on whether the BBB monolayer was exposed to 100-500 µg or 1,000 µg NPs/mL. Our calculations showed that the permeability coefficient for 50 µg/mL of IONP-PC in the transwell system with hCMEC/D3 cell layer in our study was 4×10^{-6} cm/s. Although the increase in transcytosis efficacy of IONP-PC particles compared to IONP-PEG was relatively small, we find IONP surface grafting with PC a viable strategy to design biocompatible NPs with enhanced cellular uptake properties.

Conclusions

We have examined cellular uptake and transcytosis of IONPs with an *in vitro* human BBB model employing a combination of fluorescence imaging, electrical measurement, and total reflection X-ray fluorescence. The uptake and transcytosis efficacies of IONP variants differed being dependent on surface grafting agent. This study demonstrated that, in comparison with uncoated and PEGylated IONPs, grafting of IONPs with PC brushes is a viable strategy affording comparable biocompatibility, enhanced stability, cellular uptake and improved transcytosis – all these features are desirable for MRI imaging and drug delivery and can be attributed to the natural affinity of PC – the head group of phosphatidylcholine – for the lipophilic membrane environment, plus the biomimetic property of PC. Future *in vivo* studies will be conducted to examine the biocompatibility and cellular uptake of PC-grafted IONPs.

Acknowledgements

The authors thank Ester Sporleder, Wing Yin Tong and Andrew Beck at the University of South Australia for assistance with the DLS, endothelial cell and antibody staining and cryomicrotomy, Vivian Kuusk at the Estonian University of Life Sciences for assistance with ultramicrotome preparations. This work was partly supported by ARC Project No. CE140100036 (Davis, Voelcker), Future Industries Institute of the University of South Australia (Foundation Fellowship of Ivask), Estonian Research Council grants ETF9347, PUT748 and European Regional Development Fund project TK134 (Ivask, Vija). Davis is thankful for the award of an Australian Laureate Fellowship from the ARC.

Author Contributions

A. Ivask and P. C. Ke conceived the project and wrote the manuscript. N.H. Voelcker, T.P. Davis, J.F. Quinn, M.R. Whittaker and R. Qiao provided insights to the project designs. T. Blin performed synthesis and characterizations of the IONPs. A. Ivask, H. Vija and M. Visnapuu conducted TEM, DLS, cell viability, TEER translocation and fluorescence quantification, sample preparations for hyperspectral imaging and Fe content determination, and data analysis. E.H. Pilkington conducted hyperspectral imaging and analysis. A. Käkinen performed GP analysis.

References

1. H. Arami, A. Khandhar, D. Liggitt, K.M. Krishnan, *Chem. Soc. Rev.,* 2015, **44**(23), 8576-8607.
2. R. Hufschmid, H. Arami, R.M. Ferguson, M. Gonzales, E. Teeman, L.N. Brush, N.D. Browning, K.M. Krishnan, *Nanoscale,* 2015, **7**(25), 11142-11154.
3. I. Banerjee, R.C. Pangule, R.S. Kane, *Adv. Mat.,* 2011, **23**(6), 690-718.
4. A. Ruiz, Y. Hernandez, C. Cabal, E. Gonzalez, S. Veintemillas-Verdaguer, E. Martinez, M.P. Morales, *Nanoscale,* 2013, **5**(23), 11400-11408.
5. B. Pelaz, P. del Pino, P. Maffre, R. Hartmann, M. Gallego, S. Rivera-Fernández, J.M. de la Fuente, G.U. Nienhaus, W.J. Parak, *ACS Nano,* 2015, **9**(7), 6996-7008.
6. W. Feng, S. Zhu, K. Ishihara, J.L. Brash, *Biointerphases,* 2006, **1**(1), 50-60.
7. A. Garapaty, J.A. Champion, *Chem. Commun.,* 2015, **51**(72), 13814-13817.
8. T. Cedervall, I. Lynch, S. Lindman, T. Berggård, E. Thulin, H. Nilsson, K.A. Dawson, S. Linse, *Proc. Nat. Acad. Sci. USA,* 2007, **104**(7), 2050-2055.
9. J. Cui, R. De Rose, K. Alt, S. Alcantara, B.M. Paterson, K. Liang, M. Hu, J.J. Richardson, Y. Yan, C.M. Jeffery, R.I. Price, K. Peter, C.E. Hagemeyer,P.S. Donnelly, S.J. Kent, F. Caruso, *ACS Nano,* 2015, **9**(2), 1571-1580.
10. D. Brambilla, R. Verpillot, B. Le Droumaguet, J. Nicolas, M. Taverna, J. Kóňa, B. Lettiero, S.H. Hashemi, L. De Kimpe, M. Canovi, M. Gobbi, V. Nicolas, W. Scheper, S.M. Moghimi, I. Tvaroška, P. Couvreur, K. Andrieux, *ACS Nano,* 2012, **6**(7), 5897-5908.
11. S. Schöttler, G. Becker, S. Winzen, T. Steinbach, K. Mohr, K. Landfester, V. Mailänder, F.R. Wurm, *Nat. Nanotech.,* 2016, **11**(4), 372-377.
12. K. Saha, M. Rahimi, M. Yazdani, S.T. Kim, D.F. Moyano, S. Hou, R. Das, R. Mout, F. Rezaee, M. Mahmoudi, V.M. Rotello, *ACS Nano,* 2016, **10**(4), 4421-4430.
13. B. Denizot, G. Tanguy, F. Hindre, E. Rump, J. Jacques Le Jeune, P. Jallet, *J. Colloid. Interf. Sci.,* 1999, **209**(1), 66-71.
14. K. Pu, A.J. Shuhendler, M.P. Valta, L. Cui, M. Saar, D.M. Peehl, J. Rao, *Adv. Healthc. Mat.,* 2014, **3**(8), 1292-1298.
15. J.J. Yuan, S.P. Armes, Y. Takabayashi, K. Prassides, C.A.P. Leite, F. Galembeck, A.L. Lewis, *Langmuir,* 2006, **22**(26), 10989-10993.
16. T. Blin, A. Käkinen, E.H. Pilkington, A. Ivask, F. Ding, J.F. Quinn, M.R. Whittaker, P.-C. Ke,T.P. Davis, *Polym. Chem.,* 2016, **7**(10), 1931-1944.
17. B. Weksler, I.A. Romero, P.-O. Couraud, *Fluids Barriers CNS,* 2013, **10**(1), 1-10.
18. K. Vu, B. Weksler, I. Romero,P.-O. Couraud, A. Gelli, *Eukar. Cell,* 2009, **8**(11), 1803-1807.
19. M. Pinzón-Daza, R. Garzón, P.O. Couraud, I.A. Romero, B.B. Weksler, D. Ghigo, A. Bosia, C. Riganti, *Br. J. Pharmacol.,* 2012, **167(7)**, 1431-1447.
20. S. Hanada, K. Fujioka, Y. Inoue, F. Kanaya, Y. Manome, K. Yamamoto, *Int. J. Mol. Sci.,* 2014, **15**(2), 1812.
21. J.V. Georgieva, D. Kalicharan, P.-O. Couraud, I.A. Romero, B. Weksler, D. Hoekstra, I.S. Zuhorn, *In Vitro Mol. Ther.,* 2011, **19**(2), 318-325.
22. M. Bramini, D. Ye, A. Hallerbach, M. Nic Raghnaill, A. Salvati, C. Åberg, K.A. Dawson, *ACS Nano,* 2014, **8**(5), 4304-4312.
23. M.N. Ragnaill, M. Brown, D. Ye, M. Bramini, S. Callanan, I. Lynch I, K.A. Dawson, *Eur. J. Pharm. Biopharm.,* 2011, **77**(3), 360-367.
24. D.M. Owen, C. Rentero, A. Magenau, A. Abu-Siniyeh, K. Gaus, *Nat. Prot.,* 2012, **7**(1), 24-35.
25. E.H. Pilkington, E.N. Gurzov, A. Käkinen, S.A. Litwak, W.J. Stanley, T.P. Davis, P.C. Ke, *Sci. Rep.*, 2016, **6**, 21274.
26. A.M. Schrand, J.J. Schlager, L. Dai, S.M. Hussain, *Nat. Protoc.,* 2010; **5**(4): 744-757.
27. P.B. Santhosh,A. Velikonja, Š. Perutkova, E. Gongadze, M . Kulkarni, J. Genova, K . Eleršič, A. Iglič, V. Kralj-Iglič, N.P Ulrih, *Chem. Phys. Lipids,* 2014, **178**, 52-62.
28. A.R. Mhashal, S. Roy, *PLoS ONE,* 2014, **9**(12), e114152.
29. D. Ye, M.N. Raghnaill, M. Bramini, E. Mahon, C. Aberg, A. Salvati, K.A. Dawson, *Nanoscale,* 2013, **5**(22), 11153-11165.
30. L. B. Thomsen, T. Linemann, K. M. Pondman, J. Lichota, K. S. Kim, R. J. Pieters, G. M. Visser, T. Moos, *ACS Chem Neurosci* 2013, **4**, 1352−1360
31. F. Hervé, N. Ghinea, J.-M. Scherrmann *AAPS J*, 2008, **10,** 455-472.
32. P.L. Tuma, A.L. Hubbard, *Phys Rev* 2003, **83**, 871.